Ultralight and Fire-extinguishing Current Collectors for High-energy and High-safety Lithium Ion Batteries

Authors: Yusheng Ye[1,†], Lien-Yang Chou[1,†], Yayuan Liu[1], Hansen Wang[1], Hiang Kwee Lee[1], Wenxiao Huang[1], Jiayu Wan[1], Kai Liu[1], Guangmin Zhou[1], Yufei Yang[1], Ankun Yang[1], Xin Xiao[1], Xin Gao[1], David Thomas Boyle[2], Hao Chen[1], Wenbo Zhang[1], Sang Cheol Kim[1], Yi Cui[1,3,*]

Affiliations:

[1]Department of Materials Science and Engineering, Stanford University, Stanford, California 94305, USA.

[2]Department of Chemistry, Stanford University, Stanford, California 94305, USA.

[3]Stanford Institute for Materials and Energy Sciences, SLAC National Accelerator Laboratory, 2575 Sand Hill Road, Menlo Park, California 94025, USA.

†These authors contributed equally to this work.

*Correspondence to: yicui@stanford.edu

Abstract

Inactive components and safety hazards are two critical challenges in realizing high-energy lithium ion batteries (LIBs). Metal foil current collectors (CCs) with high density are typically an integrated part of LIBs yet deliver no capacity. Meanwhile, high energy batteries can entail increased fire safety issues. Here we report a composite CC design that simultaneously minimizes the "dead weight" within the cell and improves fire safety. An ultralight polyimide-based CC (9 μm thick, specific mass 1.54 mg cm^{-2}) is prepared by sandwiching triphenyl phosphate flame-retardant embedded polyimide (PI) between two super-thin Cu layers (~500 nm). Compared to LIBs assembled with the thinnest commercial metal foil CCs (~6 μm), batteries equipped with our composite CCs can realize a 16–26% improvement in specific energy and rapidly self-extinguish fires under extreme conditions such as short circuit and thermal runaway.

Introduction

Lithium ion batteries (LIBs) are a ubiquitous technology in modern human civilization, powering devices such as portable electronics, electric vehicles and grid energy storage. The rapid development of smart devices has revitalized worldwide efforts on pursuing higher energy and safer LIBs. Commercial current collectors (CCs) are conductive metal foils made of high density materials such as copper (Cu, density 8.96 g cm^{-3}) or aluminum (Al, density 2.70 g cm^{-3}) and account for 15~50 wt.% of the total LIBs weight[1]. Although CCs in batteries play a critical role in efficient electron transfer and mechanical support for electrode materials (Fig. 1), they are generally inactive components which cause considerable "dead weight" yet do not contribute to cell capacity. Thus, the battery industry is constantly trying to decrease the thickness of those metal foils to achieve a lightweight CC. However, such attempts have demonstrated undesirable deterioration in the mechanical behavior of CCs. Recent advent of novel CCs includes 3D porous metal CC for fast battery charging[2,3], three-dimensional (3D) graphene foam for flexible LIBs[4,5], two-dimensional (2D) metal mesh for high-rate LIBs[6] and 2D carbon-based CC for LIBs[1,7,8].

However, these designs are hindered by poor mechanical behaviors, a need for additional electrolytes, high cost, poor scalability or chemical instability. Moreover, TiN coated polyimide (PI) CC has been investigated in aluminum ion batteries as a means to prevent Al CC from oxidation[9], but it is unclear how the PI composite CC affects the battery performance. In spite of those efforts made so far, the battery energy remains limited arising from the lack of lightweight and robust CC, thus calling for new approaches.

Additionally, high energy LIBs entail serious safety concerns due to the use of highly flammable organic electrolytes and polyolefin separators[10,11]. During shorting, overcharging, exposure to high temperature (> 150 °C), or other thermal abuse conditions, exothermic reactions readily occur. This release of energy, which causes separator shrinkage and the solid electrolyte interface or electrolyte to decompose, can set off a chain of additional exothermic reactions leading to thermal runaway, fires and explosions.[12-14] In addition, the breakdown of electrodes (especially metal oxide material) can exacerbate battery fires by providing an additional oxygen source[15,16]. Safe battery operation is thus a critical prerequisite for practical application of high energy LIBs. So far, considerable efforts have been dedicated to exploring safer batteries, including embedding flame-retardant materials into separators/electrolytes/electrodes, as well as the use of ceramic particle coatings[17-22]. Using such cell flame-retardants or additives can improve safety to a certain extent, but inevitably affect electron/ion transport and introduce extra weight. Replacing the electrolyte solvent with non-flammable molecules, increasing the concentration of lithium salts and adopting solid-state electrolytes can also help to formulate safe batteries[23-28]. However, these strategies generally cripple battery performance by increasing electrolyte viscosity, decreasing lithium ion conductivity, altering the operating voltage or degrading the mechanical integrity of the separator. Modified CCs with positive temperature coefficients have also been proposed to shut down the batteries when temperatures increase[29-31]. However, high leakage current, reduced electrical conductivity and increased CC weight issues in turn reduce the performance. When considering improvements of high energy LIBs, few studies have investigated simultaneously advancing performance and safety.

Here, we propose an ultralight polyimide (PI)-based CC with fire-extinguishing properties which simultaneously minimizes the "dead weight" and enhances the safety of LIBs. Our CC is fabricated by embedding triphenyl phosphate (TPP) flame-retardant into light-weight PI films, followed by coating two ultrathin external metal layers (~500 nm, Cu as an example) on both sides to impart high electrical conductivity. This CC possesses a mass loading only ~1.54 mg cm^{-2}, which is notably 7-fold lighter than normal commercial Cu foil CC. When compared to LIBs fabricated using the thinnest Cu (~6 μm thick, 5.38 mg cm^{-2}) CC, batteries assembled with our composite CCs can be improved by 16~26% in specific energy. This design isolates the flame-retardant from the LIB electron/ion pathway and chemical reactions, maintains the stability of normal cell operation and allows fast and efficient self-extinguishing of battery fires in the event of thermal runaway. Our ultralight and flame-retardant-embedded CC therefore concurrently improves specific energy and critical safety of LIBs.

CC configuration and characterization

As schematically illustrated in Fig. 1, we have selected PI as the CCs supporting film due to its low density, superior mechanical properties, good resistance to solvents, excellent thermal stability (> 400 °C) and remarkable flame resistance. The support PI film was prepared with a modified PI synthesis process utilizing pyromellitic anhydride, 4,4'-oxydianiline and 1,4-bis(4-amino-2-trifluoromethyl-phenoxy) benzene. This synthesis ensures high thermal stability (> 550

°C) compared to common PI[32,33]. The detailed synthesis process can be found in Supplementary Fig. 1. Notably, many different PIs can serve as the support substrate in this CC design, some of which are listed in the Supplementary Table 1. In order to maximize the mechanical performance of the CC, non-porous PI was synthesized[34]. Flame-retardant was mixed with PI precursor and then heated up to form composite supporting film. TPP was selected as flame-retardant material since it is one the most efficient, halogen-free, low cost, and environmental-friendly flame-retardants with a low melting point (48~50 °C)[35]. The relatively low melting point of TPP reduces the response time towards a potential fire.

Scanning electron microscopy (SEM) shows the PI structure maintains the same cross-sectional thickness of 8 μm before (Fig. 2a) and after incorporating TPP flame-retardant (PI-TPP, Fig. 2b). Here, TPP increase the uniformity of PI-TPP film. The difference in the morphology stems from the solvent-soluble feature and phase change of TPP during synthesis, whereby TPP solidifies within the PI when cooled to room temperature, as evident from the different color of PI-TPP in Supplementary Fig. 2. Besides, pre-mixing the TPP flame-retardant/PI precursors blend during synthesis contributes to a homogeneous TPP distribution. Before metal coating, we used O_2 plasma to treat the supporting film (either PI or PI-TPP), rendering the surface highly hydrophilic to enhance surface adhesion. Using magnetron sputtering deposition, two 500 nm ultrathin external metal layers (Cu as an example) are deposited on both sides to function as conductive layers (Fig. 2c) of our composite CCs (PI-Cu or PI-TPP-Cu). These metal conductive layers demonstrate good homogeneity which provides good electrical conductivity of the CC.

In contrast to previous implementation of in cell flame-retardant, our encapsulating flame-retardant in CC design eliminates potential negative impacts in electron/ion transport and side reactions. Tape peel testing reveals that the metal layer is strongly adhered to the substrate, as shown in Supplementary Fig. 3 and Supplementary Video 1. Notably, PI is cost-effective, and the metal deposition can be achieved by scalable methods, such as electroless metal plating[36] and sputtering[37]. As a proof of concept, we fabricated a PI-TPP-Cu CC with a size of 8 cm × 8 cm (Supplementary Fig. 4).

We used thermogravimetric analysis (TGA) to study the TPP content in PI-TPP with a fixed thickness of 8 μm (Fig. 2d). Specifically, TPP flame-retardant begins to decompose at ~250 °C and is completely removed from the sample by 350 °C, while the decomposition of PI mainly occurs between 550~650 °C. Based on TGA results, the contents of TPP are determined to be ~15 wt.% and 25 wt.%, which are close to the actual amount added. When the theoretical TPP content further increases to 30~50 wt.%, the TGA curves overlap and the actual TPP contents present in the PI-TPP composites remain constant at 25 wt.%, as shown in Supplementary Fig. 5. To give insight to the underlying mechanism of TPP content, X-ray photoelectron spectroscopy (XPS) depth-profiling was carried out to examine the distribution of TPP within the PI film (Supplementary Fig. 6). Prior to sputtering, no P2p XPS signal originating from TPP is detected. Subsequent sputtering of the PI-TPP film reveals the presence of TPP within the PI film, as evident from the emergence of characteristic P2p XPS peak. These results demonstrate that a surface layer of TPP may form on the composite film when excess TPP (> 25 wt.%) is added during the synthesis. The surface TPP is expected to evaporate much easier compared to the encapsulated internal TPP. Fourier-transform infrared spectroscopy (FT-IR) spectra are recorded to further confirm the existence of TPP in PI-TPP composite, as shown in Fig. 2e. The peaks at 1294 cm^{-1} can be assigned to vibrational mode of P=O in pentavalent phosphorus compounds, while the peaks of 953 cm^{-1} can be ascribed to be the P-O groups present in TPP[38].

The key factor to tune the electrical conductivity of CC relies on the conducting layers on the composite CC surfaces. Thus, we further studied the relationship between Cu thickness and resistivity of the PI-TPP-Cu CC (Fig. 2f). As Cu thickness increases, the resistivity of CC on the same side decreases due to more effective connections on the Cu conductive layer. Here, we chose 500 nm thick Cu deposition for subsequent experiments to ensure the electrical conductivity (5.71×10^7 S m^{-1}) while minimizing the weight of CC. One advantage is that we can regulate the thickness of CC by changing the thickness of PI or PI-TPP supporting film without affecting the electrical conductivity of CC as the Cu thickness is not changing. XRD patterns (Fig. 2g) demonstrate strong characteristic peaks assignable to Cu, affirming the successful Cu coating on the PI-TPP film. The dense copper coating layer can prevent TPP flame-retardant from dissolving into electrolyte.

Fig. 2h shows the specific mass of Cu foil, PI-Cu and PI-TPP-Cu CCs. Generally, a 12.0 μm and a 9.0 thick commercial Cu foil CC is ~10.75 mg cm^{-2} and 8.06 mg cm^{-2} respectively, which constitutes 25%-35% of the overall weight of an anode. Replacing Cu foil with PI-Cu CC notably reduces the mass loading of CC to 1.60 mg cm^{-2}, which is only 3~5% of the total electrode weight. Further incorporating TPP flame-retardant into PI and coating Cu on the surfaces to form PI-TPP-Cu does not obviously change the specific mass of PI-TPP-Cu CC (~1.54 mg cm^{-2}). The slightly decrease in specific mass is due to TPP (1.18 g cm^{-3}) having a lower theoretical density than PI (~1.42 g cm^{-3}). Even compared with the thinnest Cu CC (~6 μm thick, 5.38 mg cm^{-2}) used in current LIBs, our composite CC demonstrates a notable 3.5 times lighter in specific mass. Owing to the use of PI as mechanical support, our PI-TPP-Cu composite CC shows good mechanical performance (Fig. 2i). The incorporation of TPP flame-retardant into PI only slightly decrease the mechanical strength compared to that of pure PI. More interestingly, the 9.0 μm thick PI-TPP-Cu CC displays comparable mechanical behavior (Young's modulus: 2.01 GPa) compared to that of commercial Cu CC (see Supplementary Fig. 7), which is promising for practical application. Supplementary Fig. 8 depicts the overall fabrication process of PI-TPP-Cu based electrode. Various electrode materials can be coated onto our PI-TPP-Cu composite CC to form different anodic electrodes.

Fire retardancy and battery performance

We first coated graphite (Gr) electrode on commercial Cu foil and PI-TPP-Cu CC (9 μm thick) to evaluate the flame-retardancy of electrode. Vertical fire extinguishing experiment was used to evaluate the burning capacity of obtained Gr electrode. As shown in Supplementary Fig. 9, the pure PI-TPP-Cu/Gr anode does not catch fire when directly exposure to a flame. To mimic the combustion of batteries more realistically under extreme conditions, we added a pre-defined amount 1.0 M $LiPF_6$ in ethylene carbonate/diethyl carbonate (EC/DEC, 1:1 in volume) electrolyte to above electrodes and rested for 12 h to ensure complete wetting of electrolyte. Self-extinguishing time (SET) values, which describes the duration of an ignited sample continues to burn, is applied to quantify the flame retardancy. SET values are calculated by considering the mass of electrolyte maintained after resting (details in Methods).[21,22] The SET of commercial Cu CC/graphite (Cu/Gr) electrode soaked with electrolyte is ~83.3 s g^{-1}, while electrode based on PI-Cu (without TPP flame-retardant, PI-Cu/Gr) was deceased to 58.3 s g^{-1}. This is because the combustion of PI at high temperature will generate CO_2, which will in turn dilute O_2 content near the burning interface. Increasing the TPP content in PI further enhances the fire retardancy, as shown in Fig. 3a. As TPP content increases from 0 wt.% to 25 wt.%, SET time decreases linearly and achieves a small SET value of 18.0 s g^{-1}. Further increasing the added TPP amount to 50

wt.% does not obviously change the SET values, which is relevant to real TPP content, as observed during TGA results and XPS results. Considering a balance between fire retardancy and mechanical properties, we chose 25 wt.% TPP in PI-TPP as our optimized CC substrate for subsequent demonstrations.

Second, we further studied the effect of composite CC thickness on the flame retardancy. As shown in Fig. 3b, the value of SET substantially decreases when the thickness of PI-TPP-Cu increases from 5 μm to 9 μm. Even when the thickness is increased to 28 μm, the average specific mass of the PI-TPP-Cu CC is determined to be only ~3.39 mg cm^{-2} (Supplementary Fig. 10), which is still much lighter than the thinnest Cu CC (5.38 mg/cm^2, 6 μm thick) used in LIBs. In this paper, 9 μm thick PI-TPP-Cu CC was chosen for subsequent demonstrations. As shown in Fig. 3c and Supplementary Video 2, bare Cu/Gr electrode soaked with electrolyte is highly flammable and burns continuously until the electrolyte is fully exhausted. Moreover, the flame is bright and clear, demonstrating that the electrolyte is burning without any interference. For PI-Cu based graphite electrodes (PI-Cu/Gr), the flame rapidly diminishes within 2 s and is completely extinguished in 3.5 s, see Supplementary Video 3. PI-TPP-Cu based graphite electrode (PI-TPP-Cu/Gr) exhibits the best fire retardancy, whereby the flame completely self-extinguished within 1.0 s. Moreover, PI-TPP-Cu/Gr electrode appears to be burning weakly because the flame is turbid and much shorter, as shown in Supplementary Video 4. As temperature increases, TPP flame-retardant or flame-retardant radicals can be released based on the follow mechanism: (1) The mis-matched temperature coefficient of PI (3~6 × 10^{-5}/K) and Cu (~16.6 × 10^{-6}/K) will result in breakage of the original planner structure and cause cracks during thermal runaway, which will release the TPP or TPP radicals. (2) At temperature above 244 ℃ (the boiling point of TPP fire retardant), the fire retardant will be gasified and quickly released. (3) The TPP will be decomposed and generate phosphorus-containing free radicals, such as PO• and PO_2•, which then neutralize the highly active H• and HO• radicals released by the burning electrolyte or other flammable compositions[39].

Fig. 3d shows the capacities of the half cells with PI-TPP-Cu/Gr and Cu/Gr electrodes when paired with a lithium metal anode. The half cells have similar initial capacities of 412.7 and 416.2 mAh g^{-1} (based on Gr) and similar Coulombic efficiency (CE) in first activated cycle at 0.05 C, respectively. To note, many publications only report specific capacity normalized only by the weight of active materials, ignoring the heavy "dead weight" of inactivate materials in electrode[40]. Here, we compared the specific capacity of Gr electrode based on the whole mass of electrode, including active materials, CC, conductive additive and binder. As shown in Fig. 3d, the discharge capacities of PI-TPP-Cu/Gr based on whole electrode are much higher than that of Cu/Gr from 0.1 C to 1 C. At a rate of 0.5 C, the capacity of the PI-TPP-Cu/Gr retains at 226.0 mAh g^{-1} and is much higher than that of Cu/Gr electrode (146.8 mAh g^{-1}), representing a 54.0% improvement via our electrode design. Fig. 3e-f show the charge-discharge voltage profiles of the Cu/Gr and PI-TPP-Cu/Gr cells between 0.01 and 1.5 V, respectively. The voltage profiles of PI-TPP-Cu/Gr electrodes exhibit typical electrochemical features of Gr anode. Similar CE and voltage curves demonstrate that flame-retardant in our CC design does not affect battery normal operation, as further indicated in linear sweep voltammetry plots (Supplementary Fig. 11) and long cycle stability of PI-TPP-Cu/Gr anode (Supplementary Fig. 12).

Welding behaviors and pouch cell performance

Since the deposited Cu layers on the PI-Cu and PI-TPP-Cu CCs are ultrathin, it is hard to directly weld them onto a commercial Ni tab. By bridging with a Cu foil, both the PI-Cu and PI-

TPP-Cu CCs can be well welded (Fig. 4a-b). Notably, the added TPP does not affect the welding performance of designed CCs.

Traditional LIBs are assembled with Cu foil and Al foil as anodic and cathodic CC, respectively[41,42]. As a representative demonstration of commercial viability extension, we used the as-synthesized composite CCs to replace the traditional metal CCs for LIBs. 500 nm thick Cu and Al is coated on PI-based supporting film (PI or PI-TPP) as anodic CC and cathodic CC, respectively. The flame-retardant embedded cathodic CC (PI-TPP-Al) contains the same flame-retardant ratio (25 wt.%) as the anodic PI-TPP-Cu CC does because they are made from the same PI-TPP supporting film (XRD characterization of PI-TPP-Al and the fire retardancy of PI-TPP-Al/LCO are provided in Supplementary Fig. 13-14). We then constructed lithium ion full cells by coating anode and cathode on corresponding CC set: commercial Cu||Al CCs, ultralight PI-Cu||PI-Al CCs, and ultralight and fire-retarding PI-TPP-Cu||PI-TPP-Al CCs, respectively.

To mimic practical LIBs, we subsequently assembled pouch cells using the aforementioned welding method by using lithium cobalt oxide (LCO) and Gr as cathode and anode, respectively, as shown in Supplementary Fig. 15. 2 cm^2 CC areas were reserved for electrode coating. The un-used electrode area (electrode connection part) was covered by tape to avoid unwanted lithium deposition (Fig. 4c-d). We then examined the electrochemical performance of Gr-LCO full cells based on each set of CCs: Cu/Gr||LCO/Al, PI-Cu/Gr||LCO/PI-Al and PI-TPP-Cu/Gr||LCO/PI-TPP-Al. Each above abbreviation represents anodic CC/anode||cathode/cathodic CC.

Fig. 4e compares the cycle performance of different LCO-Gr full cells at a rate of 0.5 C. The Cu/Gr||LCO/Al has an ~88.1% capacity retention with stable efficiency over 200 cycles. The discharge capacities (based on LCO) of PI-Cu/Gr||LCO/PI-Al and PI-TPP-Cu/Gr||LCO/PI-TPP-Al full cells are comparable to those of Cu/Gr||LCO/Al cell. Even after 200 cycles, the capacities retention of PI-Cu/Gr||LCO/PI-Al and PI-TPP-Cu/Gr||LCO/PI-TPP-Al full cells are still maintained at ~88.0% and ~87.2%, respectively. To objectively reflect the real specific energy of batteries, we further calculated the specific energy of full cells based on the same area capacity. As can be seen from the right axis in Fig. 4e, the specific energy of traditional Cu/Gr||LCO/Al full cell is ~256 Wh kg^{-1} at initial cycle and maintains at ~226 Wh kg^{-1} after 200 cycles. Compared to traditional Cu||Al CC, the use of our ultralight composite CCs increases the specific energy of LCO-Gr LIBs to ~296 Wh kg^{-1} at initial cycles and subsequently maintains at ~261 Wh kg^{-1} after 200 cycles. These consistent cycle and high CE (Supplementary Fig. 16) of PI-TPP-Cu/Gr||LCO/PI-TPP-Al full cells highlight that TPP flame-retardant is effectively sealed in designed CC and remained stable over prolonged cycling at room temperature.

To demonstrate its potential applicability in other LIBs, we calculated the specific energy of LIBs based on different types of cathode and anode. The whole cell mass (including cathode, anode, CC, conductive additive, binder, electrolyte and separator) were considered to evaluate the potential battery specific energy based on different CCs pairs (Fig. 4f, detailed parameters and calculations are given in the Methods and Supplementary Table 2-14).

Battery specific energy is affected by CC thickness and electrode areal capacity. First, we compared the battery specific energy based on our composite CC and the thinnest Cu CC (6 μm) used so far under an areal capacity of 2 mAh cm^{-2}. As can be seen from Fig. 4f, the calculated specific energy of LIBs based on LFP, LCO, NCM111, NCM532, NCM811 and NCA when paired with Gr and Si are shown (specific abbreviations are listed below Supplementary Table 2). Replacing Cu||Al with PI-TPP-Cu||PI-TPP-Al CCs notably increases the specific energy of all

battery systems by 16~26%, which means that it is possible to achieve a specific energy higher than 400 Wh kg^{-1} based on conventional LIBs. Second, we also compared the specific energy of LIBs with different areal capacity from 2 mAh cm^{-2} to 4 mAh cm^{-2}. Even with a high areal capacity of 4 mAh cm^{-2} and the use of the thinnest CC (6 μm), an improvement of specific energy from 8% to 13% can still be achieved. More importantly, LIBs using our 9 μm thick composite CCs has a largely similar volumetric energy density, which is 99.1% of the LIBs fabricated using commercial 6 μm thick Cu CC. Our design can also be potentially extended to decrease PI-TPP-Cu thickness to 6 μm by further customizing the thickness of embedded PI-TPP layer.

Full cell fire retardancy test

Fire exposure testing is one of the most extreme safety testings in LIBs. To further investigate the performance of our PI-TPP-based CC on battery safety, we examined the fire exposure testing of Cu/Gr||LCO/Al and PI-TPP-Cu/Gr||LCO/PI-TPP-Al full cells. Pouch cells with 120 mAh of LCO cathode were paired with Gr anode and assembled as Jelly Rolls with commercial PP-PE-PP (25 μm) separators and 600 μL excessive electrolyte (Fig. 5a). The cells were sealed in the glove box and subsequently left to rest for 24 h to ensure that the electrolyte is completely soaked the cells.

By exposing the pouch cell to an open flame, the Cu/Gr||LCO/Al pouch cell immediately ignites. The flame burns vigorously and spreads rapidly throughout the entire cell, as shown in Fig. 5b and Supplementary Video 5. The pouch cell based on traditional Al/Cu CCs is completely burnt within 20 s. In contrast, the flame on the PI-TPP-Cu/Gr||LCO/PI-TPP-Al pouch cell burns weakly and rapidly self-extinguishes in about 6 s after ignition (Fig. 5c and Supplementary Video 6). More importantly, the flame appears much weaker than that of control sample. Subsequent re-burning of the pouch cells with our PI-TPP-based composite CC several times does not produce obvious flame and most of the pouch cell remains intact. The TPP flame-retardant in the pouch cell is important to impart flame-retardant property by rapidly releasing phosphate-based free radicals to suppress the fire of a burning battery. However, based on the current results, we acknowledge that a comprehensive safety testing is needed in the future.

Conclusions

In summary, we designed successfully an ultralight and self-extinguishing current collector (CC) with improved specific energy and safer characteristic for LIBs. This was achieved by replacing traditional metal foil CCs with PI-TPP-Metal composite CCs. The composite PI-TPP-Cu CC provides a four-fold decrease in density while maintaining comparable mechanical properties to that of Cu foil. The specific energy of different LIBs assembled using our CCs can be generally increased by 16~26% even compared to that using the thinnest commercial Cu||Al CCs. In contrast to previous implementation of in-cell flame-retardant, our encapsulating flame-retardant in CC design eliminates potential negative impacts in electron/ion pathway and side reactions. Our strategy on the design of next-generation CC holds enormous promise for practical battery applications by providing safer lithium batteries with even higher specific energy.

Methods

Synthesis of Pure Polyimide (PI). In a typical synthesis, N,N-Dimethylacetamide (DMAC) was used as solvent for the condensation polymerization of polyamic acid (PAA). 1,4-bis(4-amino-2-trifluoromethylphenoxy) benzene (6FAPB, 1.606 g, 3.75 mmol) and 4,4′-oxydianiline (4,4'-ODA, 0.751 g, 3.75 mmol) were added to dimethylacetamide (DMAC, 28 mL) in a 50 mL three-necked flask equipped with a mechanical stirrer, in which the molar ratio of 4,4-ODA to 6FAPB was 1:1. 4,4'-ODA is a suspected carcinogenic, which needs special attention during synthesis. After being stirred for 0.5 hour, pyromellitic dianhydride (PMDA) was added into the above solution under vigorous stirring. The molar ratio of diamines and dianhydride is 1:1.02. The reaction solution was gradually heated to 180 ºC and maintained for 2 h to complete the polymerization. The honey-like viscous PAA solution then degassed for 5 minutes to remove the gas in the solution and subsequently coated on a clean glass substrate. Doctor blading was applied to coat the solution on the glass slides with various thicknesses. The coated films were dried overnight in the fume hood at room temperature and then removed from the glass substrate by cutting the four edges of the PAA films. As-obtained free-standing PAA film was finally imidized in a box furnace under air exposure to obtain a PI film. The temperature ramping program was set as: (1) Ramp up from 25 °C to 100 °C at 3 °C min^{-1}; (2) Keep at 100 °C for 30 min; (3) Ramp up to 200 °C at 3 °C min^{-1}; (4) Keep at 200 °C for 30 min; (5) Cool down to room temperature in furnace.

Synthesis of PI-TPP. The synthesis process of PI-TPP was same with PI synthesis process except fixed amount triphenyl phosphate (TPP) flame-retardant was added to PAA solution. For 25% TPP in PI-TPP films, 0.45 g TPP was added.

Synthesis of PI-based current collectors. Before metal coating, the supporting film (either PI or PI-TPP) was treated with O_2 plasma for 5 mins to graft hydrophilic functional groups onto the surface, which increases the interfacial adhesion[43-44]. Cu layers were deposited on treated PI or PI-TPP by pulsed DC magnetron sputtering using Cu target under an argon atmosphere protection. The pressure of sputter main chamber is less than 10^{-6} Torr and the target power was set to 200 W for Cu sputtering. To obtained 500 nm thick Cu layer, a sputtering time of 1800 s was applied. Similarly, Al layers were deposited on PI-TPP film by pulsed DC magnetron sputtering using Al target under an argon atmosphere protection. The target power was also set to 200 W for Al sputtering. A series of composite anode CC (PI-Cu and PI-TPP-Cu) and composite cathode CC (PI-Al and PI-TPP-Al) were then achieved. Commercial Cu foil CC and commercial Al foil CC were used as control samples.

Electrode preparation and cell assembly. Graphite (Gr) was chosen as the anode material to estimate the performance of as-synthesized CCs. Standard slurry coating processes were applied to coat Gr onto the commercial Cu foil, PI-Cu and PI-TPP-Cu anodic CCs. Gr, super P conductive carbon and polyvinylidene fluoride (PVDF) were mixed in the weight ratio of 80:10:10 for slurry preparation with N-Methyl-2-pyrrolidone (NMP) as solvent. The slurry was degassed and filtered by 200-mesh sieves before coated on different CCs. 2032 type coin cell is used, and 11 mm-diameter electrodes were punched for the test for commercial Cu CC. To fabricate Gr electrode with PI-based CC, 11 mm-diameter supporting films (PI-Cu or PI-TPP-Cu) were punched and then sputtered Cu on the surface. The electrode slurry was then coated on the PI-based CCs. 1 M $LiPF_6$ in 50/50 (v/v) ethylene carbonate/diethyl carbonate (EC/DEC) was used as the electrolyte here. Sandwiched polypropylene-polyethylene-polypropylene (Celgard 2325) was used as separator. 750 μm thick lithium metal with a diameter of 7/16 inch was used as counter electrode. The cycling program was set as constant-current charging-discharging from 0.01 to 3.0 V (Note: Fig. 3e and 3f only show the charging-discharging curves between 0.01 and 1.5 V). LCO, Super P, PVDF in an 80:10:10 mass ratio was mixed and dispersed in NMP, then coated on commercial Al foil, PI-Al and PI-TPP-Al cathodic CCs, respectively. An initial cycle of 0.05 C was applied to optimally insert lithium ion into Gr and to form a stable SEI layer on Gr surface.

Current collector welding and LCO-Gr full cell assembling. In order to test the practical application of our composite CCs, a ~2.0 cm^2 area CC was reserved for electrode coating. LCO and Gr were chosen as cathodic and anodic active material for demonstration, respectively. Before electrode coating, the four edges of CC were covered by commercial PI films to form a controlled 2.0 cm^2 area for electrode coating. After electrodes were completely dried, the edge of PI-Cu and PI-TPP-Cu CC was welded with Ni tab by bridging with a 12 μm thick Cu film, while the edge of PI-Al and PI-TPP-Al CC was welded with Al tab by bridging with a commercial Al film. For comparison, LCO and Gr were coated on commercial Al and Cu foil, then directly welded on Al tab and Ni tab, respectively. Pouch cells were assembled based on each set of CCs: Al/LCO||Cu/Gr, PI-Al/LCO||PI-Cu/Gr, PI-TPP-Al/LCO||PI-TPP-Cu/Gr. 1 M $LiPF_6$ in 50/50 (v/v) ethylene carbonate/diethyl carbonate (EC/DEC) was used as the electrolyte for pouch cell testing. The average area capacity of active materials in these pouch cells is 3.5 mAh cm^{-2}. The pouch cells were discharged and charged between 3.0 and 4.2 V at 0.5 C using an electrochemical station

(LAND, Wuhan) to test their cycle life. For all full cells testing, 5-cycles activation was applied before cycling to form stable SEI on anodic surface.

Electrode and full cell flammability test. After Gr electrode was completely dried in a vacuum oven, we cut the electrodes into 1 cm × 5 cm strips. Vertical flame tests were performed on coated electrode materials on different CCs with a size of 1 cm×5 cm. 50 μL electrolyte was added and the electrode was sealed in 20 mL vial to make sure electrode were completely wetted by electrolyte. The fire from a gas burner was applied on the tested electrode. Self-extinguishing time (SET) values of relevant samples in consideration of the actual electrolyte mass remained in electrodes were calculated. For LCO-Gr full cell flammability test, 120 mAh pouch cells were assembled based on each set of CCs: Al/LCO||Cu/Gr and PI-TPP-Al/LCO||PI-TPP-Cu/Gr. Celgard 2325 was used as separator. After pouch cells were assembled (2.5 cm × 2.0 cm, 8 layers), 600 μL electrolyte was added and the cell was sealed to make sure the pouch cells was completely wetted by electrolyte. The mass loading of LCO and Gr in these pouch cells is ~20 mg cm^{-2} and ~12 mg cm^{-2}, respectively. In flammability test, the pouch cell with electrolyte was exposed to a direct flame from a lighter. After the cells were ignited, the lighter was removed. Then, the time for the flame to self-extinguish was recorded.

Materials Characterizations. TGA was performed on a TA Instrument Q500 with a heating rate of 5 °C/min under simulated air atmosphere (20% oxygen + 80% Argon). Fourier transform infrared (FTIR) spectroscopies were measured using an FTIR spectrometer (Model 6700, Thermo Scientific). SEM images were taken on a FEI XL30 Sirion scanning electron microscope. XPS were performed on an SSI SProbe XPS spectrometer with an Al (Ka) source. The tensile stress and strain of different films were measured using a micro materials tester (Instron, USA). Each specimen was trimmed to a 10 mm width and a 50 mm length by laser cutting to form homogenous edges, and then tested at a rate of 50 mm min^{-1}.

References

1. Chen, Y. et al. Reduced graphene oxide films with ultrahigh conductivity as Li-ion battery current collectors. *Nano Lett.* **16**, 3616-3623 (2016).
2. Zhang, H., Yu, X. & Braun, P. V. Three-dimensional bicontinuous ultrafast-charge and-discharge bulk battery electrodes. *Nat. Nanotechnol.* **6**, 277 (2011).
3. Li, Y. Q. et al. Lithium Ion Breathable Electrodes with 3D Hierarchical Architecture for Ultrastable and High-Capacity Lithium Storage. *Adv. Funct. Mater.* **27**, 1700447 (2017).
4. Li, N., Chen, Z., Ren, W., Li, F. & Cheng, H.-M. Flexible graphene-based lithium ion batteries with ultrafast charge and discharge rates. *Proc. Natl. Acad. Sci.* **109**, 17360-17365 (2012).
5. Sun, H. et al. Hierarchical 3D electrodes for electrochemical energy storage. *Nat. Rev. Mater.* 4, 45-60 (2019).
6. Liu, B. et al. Hierarchical three-dimensional ZnCo2O4 nanowire arrays/carbon cloth anodes for a novel class of high-performance flexible lithium-ion batteries. *Nano Lett.* **12**, 3005-3011 (2012).
7. Yazici, M., Krassowski, D. & Prakash, J. Flexible graphite as battery anode and current collector. *J. Power Sources* **141**, 171-176 (2005).
8. Zhamu, A., Jang, B. Z. & Chen, G. Large-grain graphene thin film current collector and secondary batteries containing same. U.S. Patent No. **9**, 484, 160 (2016).
9. Wang, S. et al. Aluminum Chloride-Graphite Batteries with Flexible Current Collectors Prepared from Earth-Abundant Elements. *Adv. Sci.* **5**, 1700712 (2018).

10. Liu, K., Liu, Y., Lin, D., Pei, A. & Cui, Y. Materials for lithium-ion battery safety. *Sci. Adv.* **4**, eaas9820 (2018).

11. Fan, X. et al. Non-flammable electrolyte enables Li-metal batteries with aggressive cathode chemistries. *Nat. Nanotechnol.* **13**, 715 (2018).

12. Wu, H., Zhuo, D., Kong, D. & Cui, Y. Improving battery safety by early detection of internal shorting with a bifunctional separator. *Nat. Commun.* **5**, 5193 (2014).

13. Liu, Y., Zhu, Y. & Cui, Y. Challenges and opportunities towards fast-charging battery materials. *Nat. Energy*, **4**, 540 (2019).

14. Liu, K. et al. Extending the Life of Lithium-Based Rechargeable Batteries by Reaction of Lithium Dendrites with a Novel Silica Nanoparticle Sandwiched Separator. *Adv. Mater.* **29**, 1603987 (2017).

15. Wang, Q. et al. Thermal runaway caused fire and explosion of lithium ion battery. *J. Power Sources* **208**, 210-224 (2012).

16. Ribière, P. et al. Investigation on the fire-induced hazards of Li-ion battery cells by fire calorimetry. *Energy Environ. Sci.* **5**, 5271-5280 (2012).

17. Yeon, D., Lee, Y., Ryou, M.-H. & Lee, Y. M. New flame-retardant composite separators based on metal hydroxides for lithium-ion batteries. *Electrochim. Acta* **157**, 282-289 (2015).

18. Yim, T. et al. Self-extinguishing lithium ion batteries based on internally embedded fire-extinguishing microcapsules with temperature-responsiveness. *Nano Lett.* **15**, 5059-5067 (2015).

19. Liu, K. et al. Electrospun core-shell microfiber separator with thermal-triggered flame-retardant properties for lithium-ion batteries. *Sci. Adv.* **3**, e1601978 (2017).

20. Yu, L., Miao, J., Jin, Y. & Lin, J. Y. A comparative study on polypropylene separators coated with different inorganic materials for lithium-ion batteries. *Front. Chem. Sci. Eng.* **11**, 346-352 (2017).

21. Baginska, M. et al. Autonomic shutdown of lithium-ion batteries using thermoresponsive microspheres. *Adv. Energy Mater.* **2**, 583-590 (2012).

22. Cui, Y. et al. A Fireproof, Lightweight, Polymer–Polymer Solid-State Electrolyte for Safe Lithium Batteries. *Nano Lett.* **20**, 1686-1692 (2020).

23. Wang, J. et al. Fire-extinguishing organic electrolytes for safe batteries. *Nat. Energy* **3**, 22 (2018).

24. Nakagawa, H. et al. Application of nonflammable electrolyte with room temperature ionic liquids (RTILs) for lithium-ion cells. *J. Power Sources* **174**, 1021-1026 (2007).

25. Zeng, Z. et al. Non-flammable electrolytes with high salt-to-solvent ratios for Li-ion and Li-metal batteries. *Nat. Energy* **3**, 674 (2018).

26. Tsujikawa, T. et al. Characteristics of lithium-ion battery with non-flammable electrolyte. *J. Power Sources* **189**, 429-434 (2009).

27. Suo, L., Hu, Y.-S., Li, H., Armand, M. & Chen, L. A new class of solvent-in-salt electrolyte for high-energy rechargeable metallic lithium batteries. *Nat. Commun.* **4**, 1481 (2013).

28. Wang, J. et al. Superconcentrated electrolytes for a high-voltage lithium-ion battery. *Nat. Commun.* **7**, 12032 (2016).

29. Xia, L., Li, S.-L., Ai, X.-P., Yang, H.-X. & Cao, Y.-L. Temperature-sensitive cathode materials for safer lithium-ion batteries. *Energy Environ. Sci.* **4**, 2845-2848 (2011).

30. Balakrishnan, P., Ramesh, R. & Kumar, T. P. Safety mechanisms in lithium-ion batteries. *J. Power Sources* **155**, 401-414 (2006).

31. Chen, Z. et al. Fast and reversible thermoresponsive polymer switching materials for safer batteries. *Nat. Energy* **1**, 15009 (2016).

32. Wang, H., Wang, T., Yang, S. & Fan, L. Preparation of thermal stable porous polyimide membranes by phase inversion process for lithium-ion battery. *Polymer* **54**, 6339-6348 (2013).

33. Ma, P. et al. A review on high temperature resistant polyimide films: Heterocyclic structures and nanocomposites. *Compos. Commun.* **16**, 84-93 (2019).

34. Li, J. et al. Synthesis and characterization of porous polyimide films containing benzimidazole moieties. *High Perform. Polym.* **29**, 869-876 (2017).

35. Velencoso, M. M., Battig, A., Markwart, J. C., Schartel, B. & Wurm, F. R. Molecular Firefighting—How Modern Phosphorus Chemistry Can Help Solve the Challenge of Flame Retardancy. *Angew. Chem. Int. Ed.* **57**, 10450-10467 (2018).

36. Kränzlin, N., Ellenbroek, S., Durán-Martín, D. & Niederberger, M. Liquid-phase deposition of freestanding copper foils and supported copper thin films and their structuring into conducting line patterns. *Angew. Chem. Int. Ed.* **51**, 4743-4746 (2012).

37. Barnat, E., Nagakura, D., Wang, P.-I. & Lu, T.-M. Real time resistivity measurements during sputter deposition of ultrathin copper films. *J. Appl. Phys.* **91**, 1667-1672 (2002).

38. Xiao, J. et al. Fire retardant synergism between melamine and triphenyl phosphate in poly (butylene terephthalate). *Polym. Degrad. Stabil.* **91**, 2093-2100 (2006).

39. Granzow, A. Flame retardation by phosphorus compounds. *Acc. Chem. Res.* **11**, 177-183 (1978).

40. Liu, N. et al. A pomegranate-inspired nanoscale design for large-volume-change lithium battery anodes. *Nat. Nanotechnol.* **9**, 187 (2014).

41. Li, M., Lu, J., Chen, Z. & Amine, K. 30 years of lithium-ion batteries. *Adv. Mater.* **30**, 1800561 (2018).

42. Schmuch, R., Wagner, R., Hörpel, G., Placke, T. & Winter, M. Performance and cost of materials for lithium-based rechargeable automotive batteries. *Nat. Energy* **3**, 267-278 (2018).

43. Hong, J. H., Lee, Y., Han, S. & Kim, K.-J. Improvement of adhesion properties for Cu films on the polyimide by plasma source ion implantation. *Surf. Coat. Technol.* **201**, 197-202 (2006).

44. Kim, M.-H. & Lee, K.-W. The effects of ion beam treatment on the interfacial adhesion of Cu/polyimide system. *Met. Mater. Int.* **12**, 425-433 (2006).

Acknowledgments:

This work was supported by the Assistant Secretary for Energy Efficiency and Renewable Energy, Office of Vehicle Technologies of the US Department of Energy under the eXtreme Fast Charge Cell Evaluation of Li-ion batteries (XCEL) program. We thank the Stanford Nano Shared Facilities (SNSF) and The Stanford Nanofabrication Facility (SNF) for SEM, FT-IR, XPS, tensile strength characterizations and Lesker sputter fabrication.

Author contributions

Y.Ye and Y.C. conceived the concept. Y.Ye, Y.C. and Y.L. designed the experiments. Y.Ye and L.C carried out the experimental works. Y.Ye and L.C. carried out the syntheses and performed material characterization, electrochemical measurements and flame retardancy tests. H.W., H.L., W.H., J.W. and K.L. assisted in the synthesis and characterization of materials. Y.Ye, Y.L., H.W., W.H., J.W., H.C., X.G. and S.C.K helped with the data analysis. Y.Yang performed the SEM experiments. H.L. helped with the X-ray photoelectron spectroscopy measurement. A.Y. collected the FT-IR spectra. X.X. helped with XRD experiments. Y.Ye and Y.C. wrote the paper. Y.Ye, W.H., G.Z, D.T.B and W.Z. revised the paper. All authors contributed to the discussion of the manuscript.

Competing interests

The authors declare no competing interests.

Additional information

Reprints and permissions information is available online at www.nature.com/reprints.

Correspondence should be addressed to Y.C.

Data availability

All relevant data are included in the paper and its Supplementary Information.

Figures

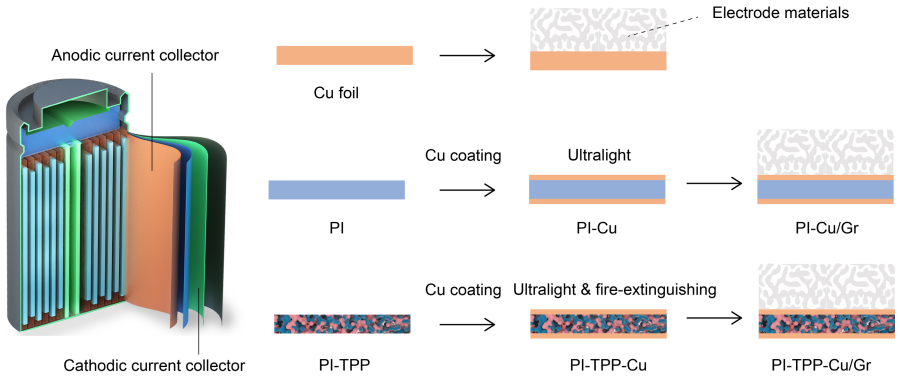

Fig. 1| Conventional current collectors and our design. Conventional pure Cu CC is heavy and bulky, while PI-Cu CC is much lighter. By incorporating with TPP flame-retardant and subsequently coating with ultrathin Cu layer on both sides, the resulting PI-TPP-Cu CC is ultralight and exhibits efficient flame retardancy properties.

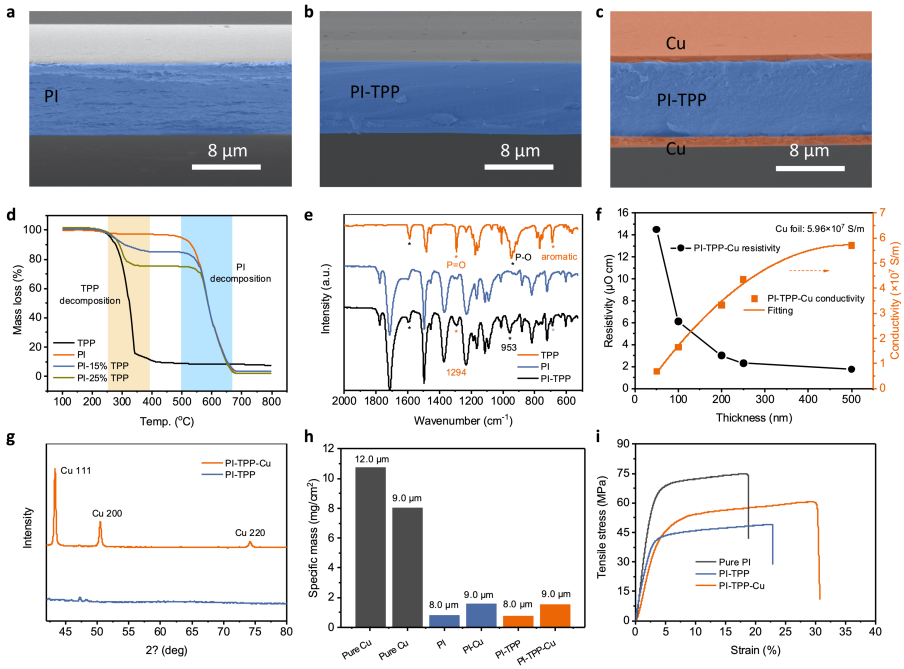

Fig. 2 | Materials fabrication and structural characterization of PI-based CCs. Cross-sectional SEM images of PI (a), PI-TPP (b) and PI-TPP-Cu (c) films. (d) TGA demonstrates the TPP contents in the PI-TPP composites. TPP flame-retardant begins to decompose at ~250 °C and is completely removed from the sample by 350 °C, while the decomposition of PI mainly occurs between 550~650 °C. (e) FT-IR spectra of the as-obtained PI, TPP and PI-TPP composite. The asterisks represent the characteristic peaks of TPP. (f) Correlation between the resistivity of CC with the thickness of Cu conductive layer. Conductivity fitting curve is obtained by polynomial fitting. When Cu thickness reaches 500 nm, the conductivity is close to that of commercial Cu foil. (g) XRD analysis on the PI-TPP and PI-TPP-Cu composites. (h) Specific mass comparison between the Cu foil, PI-TPP and PI-TPP-Cu CCs. The ultralight PI-based CC can significantly increase the specific energy of LIBs. (i) Specific tensile strength of different PI-based films.

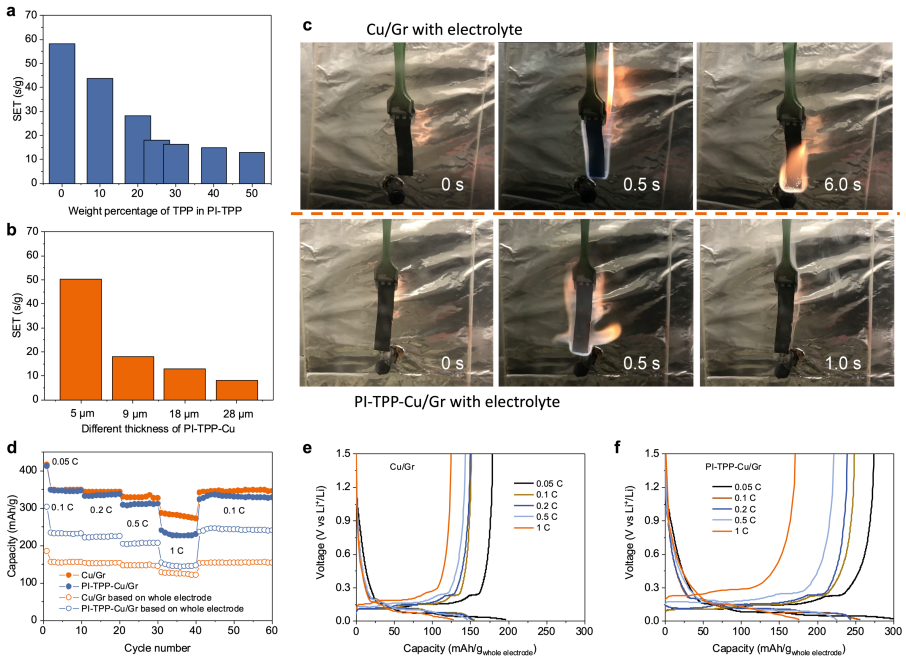

Fig. 3 | Fire retardancy behavior and Gr anode performance based on different CCs. Self-extinguishing time (SET) of the PI-TPP-Cu/Gr electrode with electrolyte for different concentrations of TPP (actual amount added) in PI-TPP (a) and different thickness of PI-TPP-Cu CCs (b). SET describes the duration of an ignited sample continues to burn. Each SET value is an average of 3 acquisitions. (c) Photographs recording the burning test of the Cu/Gr and PI-TPP-Cu/Gr electrode with electrolyte. The active material is Gr, the electrolyte is 1.0 M $LiPF_6$ in EC/DEC (1:1, v/v). Rate performance (d) and corresponding galvanostatic charge/discharge voltage profiles (e-f) of the Cu/Gr and PI-TPP-Cu/Gr electrodes between 0.01 and 1.5 V, which show that PI-TPP-Cu/Gr electrode has higher discharge capacity based on whole electrode than Cu/Gr electrode from 0.1 C to 1 C.

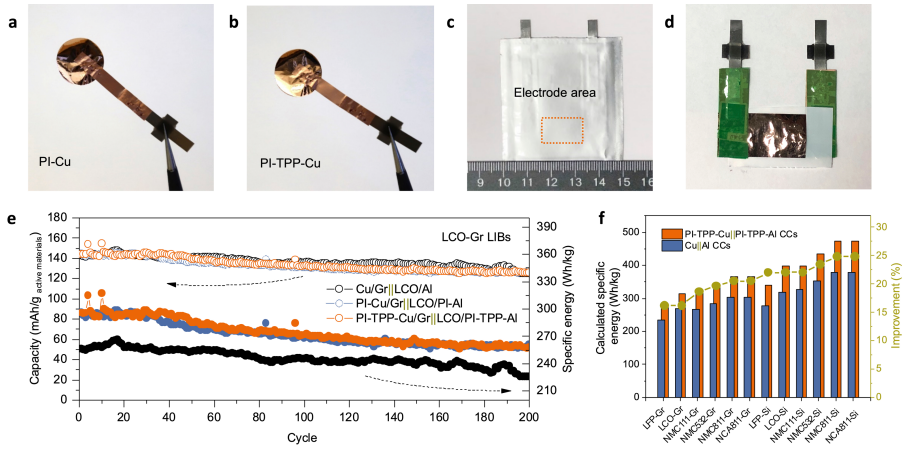

Fig. 4 | Electrochemical characterization of the full cells fabricated using conventional CCs and PI-based CCs. Digital camera photos showing the welding of PI-Cu (a) and PI-TPP-Cu (b) CCs onto copper foil. (c-d) Digital camera photos showing the pouch cell assembled using a PI-based CC. The dotted rectangle in panel c is the electrode area. (e) Galvanostatic cycling of Cu/Gr||LCO/Al, PI-Cu/Gr||LCO/PI-Al and PI-TPP-Cu/Gr||LCO/PI-TPP-Al full cells at 0.5 C. The pointing left dash arrow represents the top three curves are linked to left y axis and the pointing right dash arrow represents the bottom three curves are linked to right y axis. The open circles represent the capacity is based on cathode active materials and the filled circles repressent the capacity is based on whole mass of batteries (without packing). (f) Specific energy of different LIBs calculated based on commercial Cu||Al and PI-TPP-Cu|| PI-TPP-Al CCs. Blue and orange bars represent the specific energy ranges of batteries based on commercial Cu||Al CC pair and PI-TPP-Cu||PI-TPP-Al CC pair, respectively. The detailed cell parameters are in Supplementary Tables 2-14.

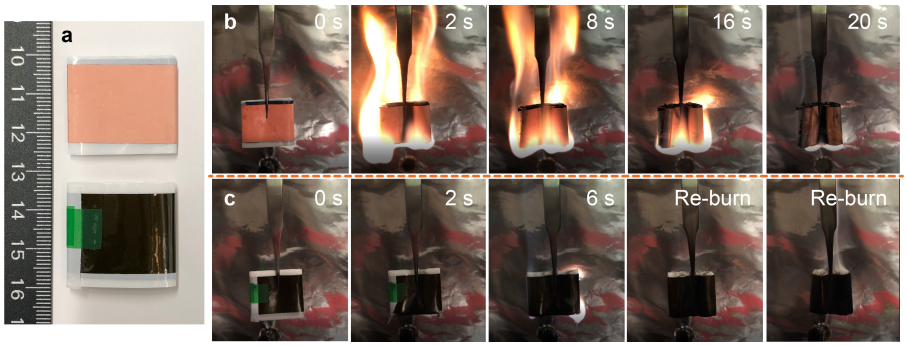

Fig. 5 | Fire retardancy test on full pouch cells assembled by Al/Cu CC pair and PI-TPP-Al/PI-TPP-Cu CC pair. (a) Photos of the assembled Cu/Gr||LCO/Al (top) and PI-TPP-Cu/Gr||LCO/PI-TPP-Al (bottom) pouch full cells. Flame retardancy test results for the Cu/Gr||LCO/Al (b) and PI-TPP-Cu/Gr||LCO/PI-TPP-Al (c) pouch full cells.